Available online at www.sciencedirect.com
SCIENCE DIRECT®
Journal of Magnetic Resonance 166 (2004) 228–235
JMR Journal of Magnetic Resonance
www.elsevier.com/locate/jmr

3D imaging with a single-sided sensor: an open tomograph

J. Perlo, F. Casanova, and B. Blümich*

Institut fürTechnische und Macromolekulare Chemie, RWTH Aachen D-52056, Germany

Received 29 August 2003; revised 22 October 2003

Abstract

An open tomograph to image volume regions near the surface of large objects is described. The central achievement in getting such a tomograph to work is the design of a fast two-dimensional pure phase encoding imaging method to produce a cross-sectional image in the presence of highly inhomogeneous fields. The method takes advantage of the multi-echo acquisition in a Carr–Purcell–Meiboom–Gill (CPMG)-like sequence to significantly reduce the experimental time to obtain a 2D image or to spatially resolve relaxation times across the sensitive volume in a single imaging experiment. Depending on T_2 the imaging time can be reduced by a factor of up to two orders of magnitude compared to the one needed by the single-echo imaging technique. The complete echo train decay has been also used to produce T_2 contrast in the images and to spatially resolve the T_2 distribution of an inhomogeneous object, showing that variations of structural properties like the cross-link density of rubber samples can be distinguished by this method. The sequence has been implemented on a single-sided sensor equipped with an optimized magnet geometry and a suitable gradient coil system that provides two perpendicular pulsed gradient fields. The static magnetic field defines flat planes of constant frequency parallel to the surface of the scanner that can be selected by retuning the probe frequency to achieve slice selection into the object. Combining the slice selection obtained under the presence of the static gradient of the open magnet with the two perpendicular pulsed gradient fields, 3D spatial resolution is obtained.

Keywords: MRI; Unilateral NMR; Mobile probes; NMR-MOUSE

1. Introduction

Single-sided NMR sensors are used to characterize large size objects by measuring relaxation times and self-diffusion coefficients inside a spot near the surface or sensitive volume generated in the sample by an open magnet [1]. Different tool geometries have been designed and optimized depending on the application for material analysis and quality control [2,3], well logging investigation [4,5], water reservoir studies [6], moisture detection in composites [7], and medical diagnostics [8,9].

To assess the degree of heterogeneity of samples across the sensitive volume, imaging methods are required. Achieving spatial resolution with a single-sided probe converts the tool in a truly non-invasive open tomograph. In the last years special effort has been made to develop new imaging techniques to be used in the presence of the strongly inhomogeneous magnetic fields generated by open magnet geometries [10–12] and the stray field of superconducting magnets [13]. A hand held design of a unilateral sensor that has been extensively used for materials testing is the so-called NMR-MOUSE (mobile universal surface explorer) [2]. Recently, two-dimensional images have been obtained implementing a single-point imaging method on a NMR-MOUSE equipped with a dedicated gradient coil system to produce two perpendicular pulsed gradient fields [11]. The principal limitation of the method for 3D imaging was the long experimental time, of the order of 1 h, necessary to obtain a 2D image with a resolution of 1 mm at 1 mm depth.

Recently we have reported a fast imaging technique that takes advantage of the multi-echo acquisition in a Carr–Purcell–Meiboom–Gill (CPMG) sequence to improve the sensitivity of a 1D imaging experiment [12]. The basic idea to speed up data acquisition relies on the fact that the echo time T_E used for the Hahn-echo sequence is usually much shorter than the T_2 of the sample, and a train of echoes can be generated by applying a

* Corresponding author. Fax: +49-241-8022185.
E-mail address: bluemich@mc.rwth-aachen.de (B. Blümich).

1090-7807/$ - see front matter © 2003 Elsevier Inc. All rights reserved.
doi:10.1016/j.jmr.2003.10.018

CPMG sequence. As it was demonstrated, the extension from a single- to a multi-echo imaging experiment is not straightforward because the off-resonance excitation introduces significant distortions in the phase encoding defined by the gradient pulses. To overcome this distortion independent phase encoding was performed on each echo similar to the RARE method [14], applying two gradient pulses with opposite polarization before and after the echo formation.

In this work we propose a new multi-echo sequence to produce a cross-section of a selected slice. It is composed of a first encoding period, where both gradient pulses are applied to achieve lateral resolution, followed by a train of refocusing pulses for multi-echo acquisition. Compared to the previously published version this sequence minimizes the power dissipated by the gradient coil system and increases the sensitivity improvement by maximizing the number of echoes acquired during the train. This technique has been implemented in an optimized U-shaped magnet design that provides a large volume where the static magnetic field defines planes of constant frequency parallel to the scanner surface. Under the strong gradient of the static field, hard radio-frequency (RF) pulses produce selective excitation of thin flat slices at different depths into the object selected by changing the excitation frequency.

The imaging method and the sensor, including the magnet geometry and the gradient coil system are described in the next sections. The technique was applied to improve the signal-to-noise in a 2D imaging experiment. Using a silicon rubber sample with long T_2 a considerable sensitivity improvement was achieved and a complete 2D image was acquired with a single scan per gradient step. In another application, the sequence was used to measure the T_2 distribution of an inhomogeneous object spatially resolved across the sensitive volume. Instead of adding the echo in the CPMG train a 2D image was reconstructed from each echo, and fitting each pixel decay as a function of the number of echoes the local T_2 was obtained. In a third application, the method was used to obtain a set of 2D images selecting slices at different depths showing that 3D spatial localization can be achieved with this sensor.

2. Method

The pulse sequence for multi-echo acquisition is depicted in Fig. 1. It is divided into an encoding and a detection period. A first Hahn-echo sequence is used to refocus the magnetization spread introduced by the static field inhomogeneities while both pulsed gradients, applied in the first free evolution interval, encode position in the phase of the echo signal. Following the spatial encoding period a detection subsequence composed of a train of refocusing pulses is applied to generate a train of echoes. The encoding echo time T_{EE} is determined by the length of the gradient pulses, but the detection echo time T_{ED} is limited only by the dead time of the probe. In this way the generated number of echoes is maximized increasing the sensitivity improvement.

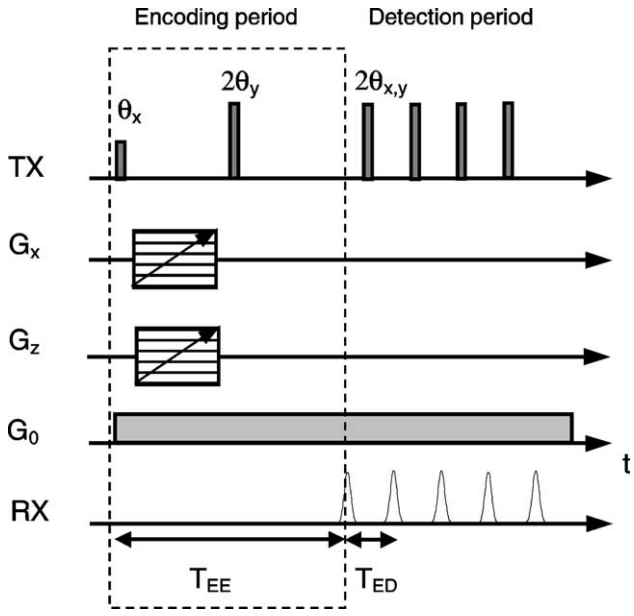

Fig. 1. New multi-echo sequence applied to sample the complete echo decay train. Both gradient pulses are applied simultaneously after the first RF pulse and determine the encoding echo time T_{EE} of the first Hahn-echo sequence. To maximize the number of echoes that can be generated during the detection period, the echo time is reduced after the formation of the first echo. The detection echo time T_{ED} is determined by the dead time of the probe.

The spin dynamics during the application of this pulse sequence in the presence of a grossly inhomogeneous B_0 and B_1 fields can be understood following the analysis by Hurlimann and Griffin [15]. They have extensively analyzed the evolution of the magnetization over the application of a pulse sequence composed by an initial excitation period $\boldsymbol{A}$ followed by identical refocusing cycles $\boldsymbol{B}$, where both can consist of any number of RF pulses and free evolution periods. In the standard CPMG sequence $\boldsymbol{A}$ is the nominal $(\pi/2)_x$ RF pulse and $\boldsymbol{B}$ consist of a period τ of free precession, a nominal $(\pi)_y$ RF pulse, followed by another free precession period τ. When the subsequence $\boldsymbol{B}$ is symmetric like the one in the CPMG sequence, a preferential direction in the rotating frame contained in the plane defined by the static field and the direction of the refocusing RF pulses is defined. When the refocusing pulses are applied along the y axis, the component of the magnetization created by the subsequence $\boldsymbol{A}$ parallel to this preferential direction is locked during the train preserving only the y component of the echo signal, while the x component goes to zero after a transient period.

In the imaging sequence shown in Fig. 1, $\boldsymbol{A}$ is the first Hahn-echo sequence and the initial state for the

subcycles $\boldsymbol{B}$ is the peak of the first echo. The gradient pulses applied after the first RF pulse fan out the magnetization in the plane encoding the position in the phase of the echo signal. For image reconstruction both magnetization components are necessary, and the loss of one of them mirrors the spectrum. To sample both components two experiments must be performed switching the direction of the RF pulses of the refocusing train from x to y. The full complex signal is then built by combining the x component of the first train with the y component of the second.

3. Experimental

A drawing of the unilateral sensor including the magnet, the gradient coil system and the RF coil built for this work is depicted in Fig. 2. A U-shaped magnet with an optimized field profile [16] that generates flat slices of constant frequency perpendicular to the depth direction was used to provide the static magnetic field. The three magnetic field components were scanned with a Lake Shore 420 Hall probe at three different positions above the magnet (Fig. 3). The shape of the field is curved at the surface of the magnet (where the field is the strongest), but becomes quite flat for higher depths (Fig. 3A).

The field intensity is rather constant along x for each depth, but along the z direction it starts parabolic at the surface reducing its curvature as a function of the distance from the magnet surface (Fig. 3B). To calculate the deviation from a flat slice along both x and z directions the value of the static field gradient is needed. Fig. 3C shows the field variation along the y direction scanned at the center of the magnet. In the region between 25 and 45 mm from the magnet surface it possess a constant gradient along y of about 2.5 T/m.

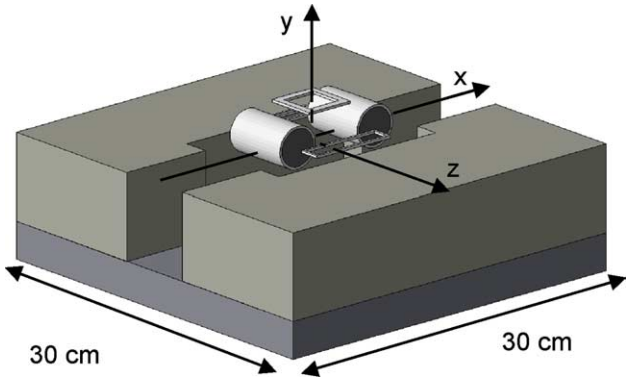

Fig. 2. Drawing of the single-sided sensor built for this work. It shows the geometry of the U-shaped magnet, the gradient coil system and RF coil used for the open tomograph. This magnet geometry produces a static field with a main component along z. Two solenoids 34 mm diameter, 54 mm long and separated by 74 mm from center to center generate G_x, while two rectangular coils $17 \times 70\,\text{mm}^2$, separated by 75 mm from center to center, provide G_z. A 40 mm squared RF coil is positioned at 30 mm above the magnet. Both gradient coils pairs are placed with their center at 10 mm from the magnet surface. The origin of the coordinates system is on the upper side in the center of the magnet.

Using it as an average gradient value and assuming the gradient is predominantly along the y direction, the variation of the static field across the slice can be used to estimate its curvature. It can be noticed that the flatness of the slices depends on the lateral dimension of the excited volume along both x and z directions, obtaining the best results when operating as close as possible to the center at $x = z = 0$. For our purposes a lateral field-of view of $20 \times 20\,\text{mm}^2$ and a slice deviation smaller than half a millimeter are desired. It is fulfilled for depths starting at $y = 30$ mm and larger, where the field variation between $z = 0$ and $z = \pm 10$ mm is 1 mT. The field variation along x is always much smaller than the one along z, defining a field of view (FoV) of 40 mm at $y = 30$ mm. To maximize the sensitivity the object was positioned at the highest frequency where the slice was sufficiently flat. This plane was found at $y = 30$ mm where the resonance frequency is 8.35 MHz.

The selection on the x–z plane is achieved by the RF coil, which was designed to assure the desired quality in the slice selection. For excitation and detection of the NMR signal, a 40 mm squared, four-turn RF coil was wound from 2 mm diameter copper wire. For the loaded circuit Q is about 45 and the dead time is 40 μs. The probe can be manually tuned between 8.35 and 7.35 MHz covering a range of 10 mm depth. The coil was located at 30 mm above the surface of the magnet. This defines the sensor surface at this position. The decay of the RF field along y was measured in order to compensate the B_1 reduction by increasing the output of our linear power amplifier. The lateral selection of this coil is shown in the next section.

The gradient coil system built to provide two perpendicular pulsed gradients along the x and z axes was positioned inside the gap between the magnets and underneath the RF coil (Fig. 2). Two solenoids, 34 mm in diameter and 54 mm long, separated by 74 mm from center to center, and wound in anti-parallel configuration, generate a pulsed magnetic field with a constant gradient along the x direction. To provide a pulsed gradient along the z axis, two rectangular coils $17 \times 70\,\text{mm}^2$, separated by 75 mm from center to center, and wound in parallel configuration were built. The position of these coils was optimized to generate uniform gradients in the first centimeter of depth. The intensity variation of both gradients along the depth direction was calibrated in order to compensate for the reduction of the gradient efficiency and keep the field of view fixed. Two model 7541 Techron amplifiers delivering a maximum voltage of 60 V and a maximum current of 20 A, were used to drive the coils. The maximum gradient available at the surface of the sensor is 40 and 24 mT/m along x and z directions, respectively.

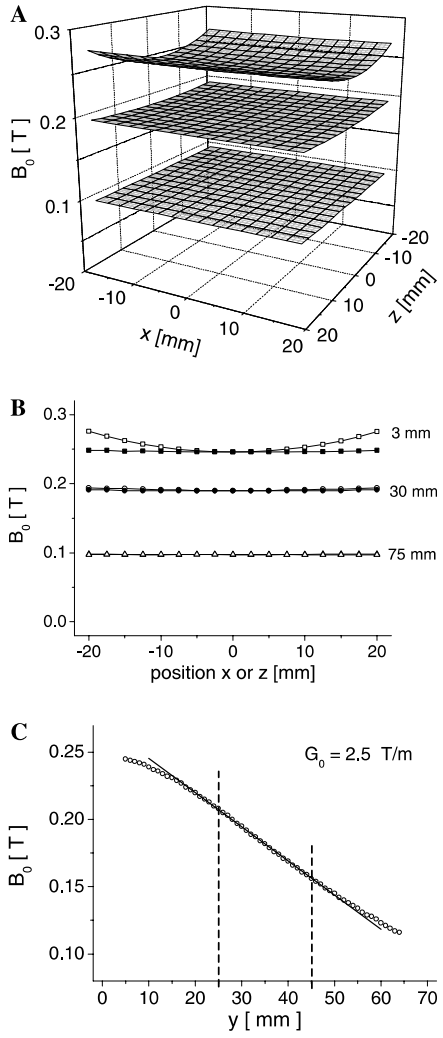

Fig. 3. (A) Magnetic field intensity scanned at 0, 30, and 75 mm from the magnet surface. The field profile is curved at the surface and reaches a flat shape at 30 mm. (B) One-dimensional field profiles along the x (solid) and z (open) axes for the three scanned positions. The field is almost constant along the x axis at every position but it is curved along the z axis. (C) Dependence of the field intensity along the y direction, the static field has a constant gradient of about 2.5 T/m between 25 and 45 mm.

4. Result

4.1. Sensitivity improvement

The time reduction factor that can be achieved using the new multi-echo technique instead of the Hahn-echo sequence becomes significant for samples having long T_2. To show the improvement with the new sequence a sample was cut from a silicone rubber with a $T_1 = 330$ ms and $T_2 = 90$ ms (Fig. 4A). It was positioned above the RF sensor and a 1 mm thick slice at 5 mm depth was selected. The sequence of Fig. 1 was applied using gradient pulses 0.37 ms long and an echo time T_{ED} of 0.11 ms. The gradient amplitude was increased in 32 steps sampling k space from negative to positive values. The field of view (FoV) was set to 32 mm along both directions to obtain a spatial resolution of about 1 mm.

A single scan was used per gradient amplitude, and 800 echoes were acquired and averaged to improve the signal-to-noise ratio. It is important to point out that two experiments are needed per gradient amplitude to acquire both the x and y components of the echo signal. A recycling delay of 0.45 s was used between experiments resulting in a total experimental time of 15 min to obtain a 2D image. Fig. 4B shows the cross-section obtained using the new pulse sequence. The image reproduces the structure of the object without appreciable distortions showing that 2D spatial localization can be obtained across the selected slice.

To obtain a 2D cross-section with the same signal-to-noise ratio but using the single-echo sequence a larger number of scans must be used. As the intensity of the echo train decays exponentially and it is sampled up to one-third of its initial intensity the sensitivity improvement can be easily calculated. For this rubber sample 175 full Hahn-echoes must be averaged to obtain the signal-to-noise ratio provided by the multi-echo sequence, giving a experimental time of about 43 h.

The new fast imaging method offers also important advantages in sensitivity and power dissipation over the previously published multi-echo sequence. The old sequence requires the application of gradient pulses before and after each echo formation, and it limits the minimum echo time to 0.8 ms reducing the number of echoes generated by the sequence from 800 to 60. Table 1 gives the comparison of the experimental time needed, and the average power and total energy dissipated by both multi-echo sequences and the Hahn-echo method. The new multi-echo version not only offers the highest sensitivity but also tremendously reduces the total energy required to run a 2D imaging experiment, which represents an important issue determining the

Table 1
Comparison between the single-echo, RARE, and the multi-echo imaging methods

Sequence	Experimental time	RF power (W)	Gradient power (W)	Energy (kJ)
Hahn-echo	43 h	0.002	0.4	62
RARE	100 min	0.1	47	282
New multi-echo	15 min	1.4	0.4	1.6

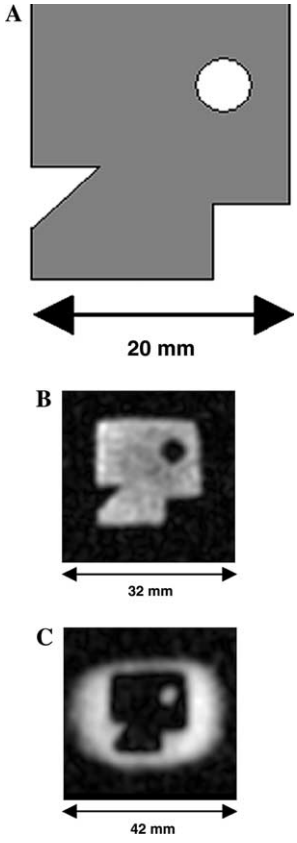

Fig. 4. (A) Geometry of a test object made of silicon rubber. (B) Two-dimensional image obtained by applying the new multi-echo acquisition scheme. Thanks to the 800 echoes generated during the echo train decay, a single scan per gradient amplitude was needed to sample each quadrature channel. The echo train was sampled until the amplitude had decayed to 30% of the initial amplitude and before adding the echo train it was apodizated by the same decay function. The total experimental time to obtain the 2D images with a spatial resolution of about 1 mm was 15 min, reducing the acquisition time by a factor of 175 compared to the single-echo method, which would require 43 h. (C) Subtraction of the image (B) from the image of a uniform object $50 \times 50\,\mathrm{mm}^2$ used to probe the FoV defined by the RF coil. The dimensions of the selected sensitive volume are 36 mm along x and 26 mm along z.

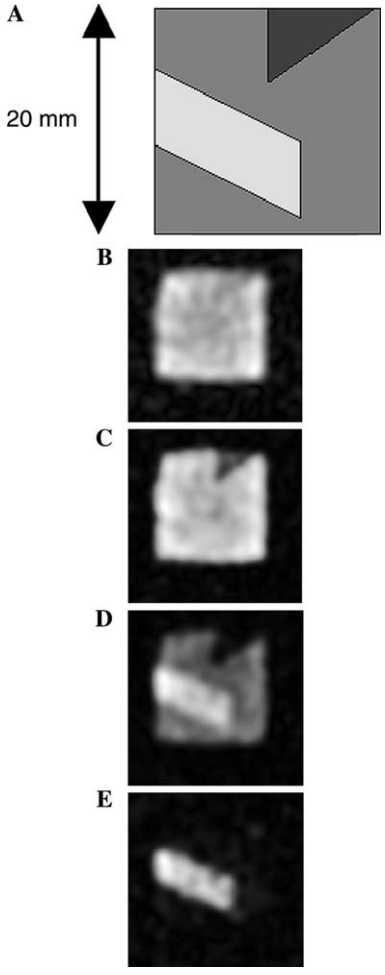

Fig. 5. (A) Object geometry composed of three different kinds of rubber presenting different relaxation times. To produce different T_2 contrast different train intervals were averaged before imaging reconstruction. The images obtained by adding (B) the echoes 0–8, (C) 8 –32, (D) 100–200, and (E) 200–400 show different intensity ratios between the three regions.

autonomy for portable systems where the energy is stored in batteries.

The field of view defined by the RF coil was probed by a uniform silicon rubber sample with dimensions $50 \times 50\,\mathrm{mm}^2$ along the x and z axes. The fast imaging method was implemented using the parameters of the previous experiment, but a FoV of 42 mm was set. Fig. 4C shows the result obtained by subtracting the image of Fig. 4B from the image of the uniform object. The RF coil defines a FoV of 36 mm along x and 26 mm along z. In case a large object is positioned on the sensor the FoVs must be set larger than these dimensions to avoid folding of the signal. For the sake of simplicity, objects with limited sizes along x and z will be used from this point on.

4.2. Spatially resolved relaxation times

As a second application, the multi-echo imaging sequence was used to spatially resolve the T_2 distribution of an inhomogeneous object. Three different rubber samples with different relaxation times were used to build the object shown in Fig. 5A. A 1 mm thick slice at 5 mm from the surface and inside the object was selected. The multi-echo sequence was applied setting $T_{ED} = 0.11$ ms and using 1000 echoes to correctly sample the longest decay present in the object. The gradient amplitude was increased in 24 steps, and with the FoV set to 32 mm a spatial resolution of about 1.3 mm was obtained. The repetition time was set to 0.3 s, 3 times the longest T_1 to avoid any T_1 weighting in the image. Eight scans were averaged for sensitivity improvement.

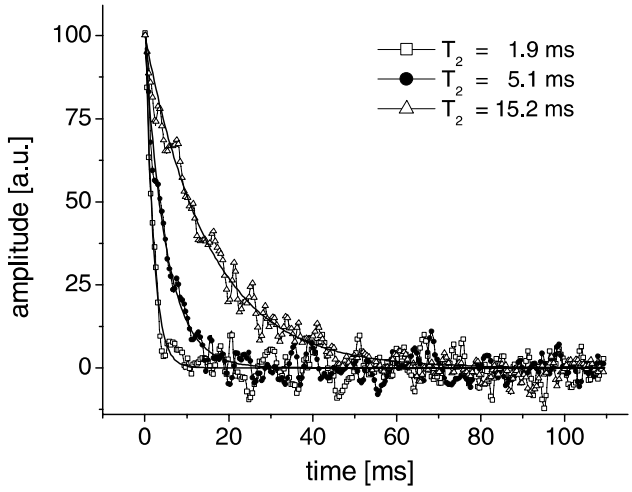

Fig. 6. Amplitude decays correspondent to the three characteristic regions inside the object. Fitting the decaying signal in each pixel the local relaxation time was obtained. The values shown in the picture are in agreement with the relaxation times of each rubber sample.

Fig. 5 shows different T_2 weighted images reconstructed from the addition of the echoes (B) 0–8, (C) 8–32, (D) 32–200, and (E) 200–400. Normalizing the highest intensity of each image to one, Fig. 5B shows the rectangular object with almost uniform intensity, Fig. 5C shows the shortest T_2 region with half of the maximum intensity, while the other two regions cannot be differentiated, Fig. 5D shows the shortest T_2 with zero intensity, the second one with the half of the intensity, and the longest with full intensity, and finally in Fig. 5D only the region with the longest T_2 is visible.

Instead of adding parts of the echo train to produce contrast in the images the local relaxation time can be obtained by fitting the intensity decay of each pixel. In contrast with the single-echo method the complete decay is sampled in a single imaging experiment, reducing the dimensionality of the experiment by one. Fig. 6 shows the signal decays corresponding to each region in the object together with the respective fit. From dark to light gray the obtained relaxation times are 1.9, 5, and 15 ms, in agreement with the relaxation times measured from each single rubber sample using a CPMG sequence.

4.3. 3D spatial localization

Combining the 2D phase encoding method with slice selection, 3D spatial resolution is achieved. Fig. 7 shows an object with a 3D structure obtained by stacking a set of letters forming the word MOUSE cut from a sheet of 2 mm thick natural rubber. Having no spacer in between the letters an object 10 mm high is

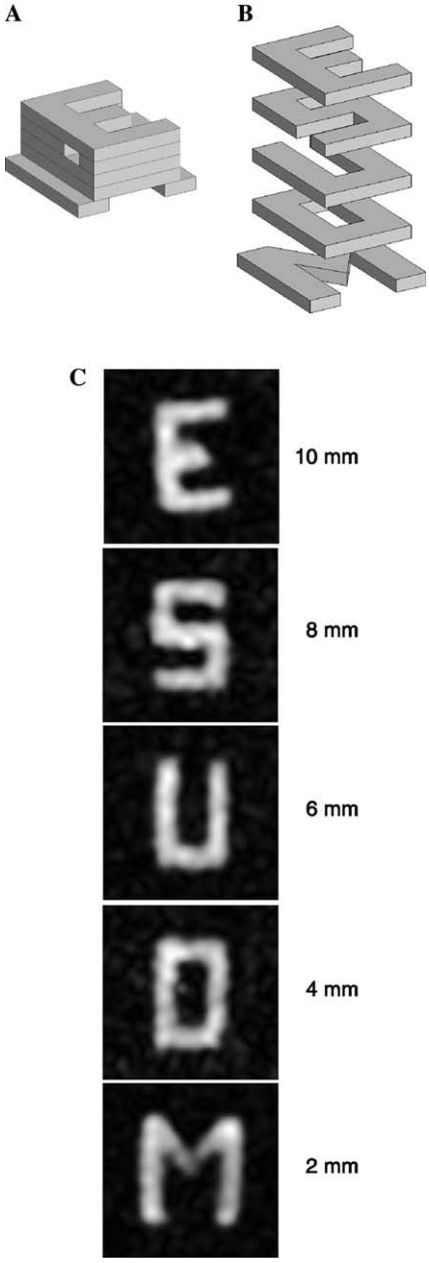

Fig. 7. (A) Object made staking the letters of the word MOUSE cut from a rubber sheet 2 mm thick. The object was placed inside a holder with 1 mm walls. (B) Expanded view of the object obtained by drawing the letters separate from each other to see the object structure. (C) Images of each letter obtained applying the multi-echo imaging method and selecting a 1 mm thick slice in the center of each letter. To compensate for the loss in sensitivity due to the B_1 decay, the number of scans used for each letter was increased with the depth. The total time to obtain each letter was 45, 45, 90, 120, and 180 s, respectively.

obtained. For a better view Fig. 7B shows the letters separated one from the other. After calibrating the frequency dependence with the position along the depth direction different 1 mm thick slices were selected one inside each letter. The new multi-echo

acquisition scheme was applied using 20 gradient steps and a FoV of 32 mm, giving a spatial resolution of about 1.6 mm. To have the same FoV at different depth both gradient intensities were calibrated. For this rubber sample 96 echoes were added for sensitivity improvement. Using a recycle delay of 30 ms and 2 scans an experimental time of 48 s was needed to obtain the image of the first letter. To compensate the loss of sensitivity due to the B_1 reduction as a function of depth, an increasing number of scans was used for the next letters needing a factor of four for the last letter. The 2D images of each letter can be observed in Fig. 7C. The flatness of the sensitive volume is good enough to observe no superposition of consecutive letters, and as no distortions can be observed in any of them we conclude the uniformity of the pulsed gradients is acceptable in the complete range.

5. Conclusion

A pure phase encoding multi-echo imaging method was presented to produce 2D images reasonably quickly in strongly inhomogeneous magnetic field. The sequence was implemented on a single-sided NMR sensor equipped with a gradient coil system to produce pulsed gradients along two perpendicular space directions. The multi-echo feature of the technique was applied to reduce the imaging experimental time and to spatially resolved T_2 distributions across an inhomogeneous object. Not only density images could be obtained in experimental times under 1 min but T_2 weighted images to distinguish heterogeneities inside the object were also produced. The combination of the new two-dimensional imaging method with slice selection provided by the static gradient gives truly non-invasive 3D imaging capabilities with an open tomograph that can be used for material analysis and quality control of arbitrarily large samples.

The important innovation is the demonstration that generating multiple echoes and co-adding them achieves a dramatic reduction in measurement time. Previously only the feasibility of obtaining 3D images from a stack of multiple slice selective images has been shown [11] but the acquisition times were prohibitive, and the idea of adding multiple echoes for reducing the measurement has been stated in context with unilateral NMR but not verified experimentally [17]. An added benefit of the method is the considerable savings in total energy. This feature is particularly important for mobile applications. Clearly, the same method can be used in other stray-field imaging applications [13,18]. It is anticipated, that the new unilateral imaging sensor will find applications in non-destructive quality control and product failure analysis, where it can be employed similar to a magnifying glass which is capable of looking inside a large object at a selected spot. While in this work the RF has been changed manually for slice selection, in future applications is can be changed electronically by switching the tuning elements of the RF circuit [19].

Acknowledgments

Federico Casanova thanks the Alexander von Humboldt foundation for a research scientist fellowship. Support of this project by the DFG Forschergruppe FOR333 surface NMR of Elastomers and Biological Tissue is gratefully acknowledged.

References

[1] R.L. Kleinberg, A. Sezginer, D.D. Griffin, M. Fukuhara, Novel NMR apparatus for investigating an external sample, J. Magn. Reson. 97 (1992) 466–485.
[2] G. Eidmann, R. Salvelsberg, P. Blümler, B. Blümich, The NMR-MOUSE, a mobile universal surface explorer, J. Magn. Reson. A 122 (1996) 104–109.
[3] G.A. Matzkanin, A review of non-destructive characterization of composites using NMR, in: Nondestructive Characterization of Materials, Springer, Berlin, 1998, p. 655.
[4] R.L. Kleinberg, Well logging, in: D.M. Grant, R.K. Harris (Eds.), Encyclopedia of NMR, Wiley, New York, 1996, pp. 4960–4969.
[5] J.A. Jackson, L.J. Burnett, F. Harmon, Remote (inside–out) NMR. III. Detection of nuclear magnetic resonance in a remotely produced region of homogeneous magnetic field, J. Magn. Reson. 41 (1980) 411–421.
[6] O.A. Shushakov, Ground water NMR in conductive water, Geophysics 61 (1996) 998–1006.
[7] P.J. Prado, NMR hand-held moisture sensor, Magn. Reson. Imaging 19 (2001) 505–508.
[8] US Patent 5,959,454. Bruker Analytic. Magnet arrangement for an NMR tomography system, in particular for skin and surface examinations.
[9] R. Haken, B. Blümich, Anisotropy in tendon investigated in vivo by a portable NMR scanner, the NMR-MOUSE, J. Magn. Reson. 144 (2000) 195–199.
[10] P. Prado, B. Blümich, U. Schmitz, One-dimensional imaging with a palm-size probe, J. Magn. Reson. 144 (2000) 200–206.
[11] F. Casanova, B. Blümich, Two-dimensional imaging with a single-sided NMR probe, J. Magn. Reson. 163 (2003) 38–45.
[12] F. Casanova, J. Perlo, B. Blümich, K. Kremer, Multi-echo imaging in highly inhomogeneous magnetic fields, J. Magn. Reson., in press.
[13] J. Godward, E. Ciampi, M. Cifelli, P.J. McDonald, Multidimensional imaging using stray field pulsed gradients, J. Magn. Reson. 155 (2002) 92–99.
[14] B. Blümich, in: NMR Imaging of Materials, Oxford University Press, Oxford, 2000, p. 222.

[15] M.D. Hürlimann, D.D. Griffin, Spin dynamics of Carr–Purcel–Meibohm–Gill-like sequences in grossly inhomogeneous B_0 and B_1 fields and applications to NMR well logging, J. Magn. Reson. 143 (2000) 120–135.
[16] H. Popella, G. Henneberger, Modelling and optimization of the magnetic circuit of a mobile NMR device for MRI, J. IEEE Trans. Magn., 2003, in press.
[17] US Patent 5,767,675. Panacea Medical Laboratories. Mixed timing CPMG sequence for remotely positioned MRI.
[18] P.J. McDonald, Stray field magnetic resonance imaging, Prog. Nucl. Magn. Reson. Spectrosc. 30 (1997) 69–99.
[19] P.J. Prado, Single sided imaging sensor, Magn. Reson. Imaging 21 (2003) 397–400.